Research Paper
J. Astron. Space Sci. 33(4), 313-318 (2016)
http://dx.doi.org/10.5140/JASS.2016.33.4.313

JASS Journal of Astronomy and Space Sciences

Edge Detection Method Based on Neural Networks for COMS MI Images

Jin-Ho Lee†, Eun-Bin Park, Sun-Hee Woo
Korea Aerospace Research Institute, Daejeon 34133, Korea

Communication, Ocean And Meteorological Satellite (COMS) Meteorological Imager (MI) images are processed for radiometric and geometric correction from raw image data. When intermediate image data are matched and compared with reference landmark images in the geometrical correction process, various techniques for edge detection can be applied. It is essential to have a precise and correct edged image in this process, since its matching with the reference is directly related to the accuracy of the ground station output images. An edge detection method based on neural networks is applied for the ground processing of MI images for obtaining sharp edges in the correct positions. The simulation results are analyzed and characterized by comparing them with the results of conventional methods, such as Sobel and Canny filters.

Keywords: COMS MI image, edge detection, neural network, SNN, Sobel filter

1. INTRODUCTION

On receiving image data obtained from Communication, Ocean And Meteorological Satellite (COMS) meteorological imager (MI), the ground station initiates the process of radiometric and geometric correction. When performing the radiometric process, by applying gains and offsets to their pixel values, the raw image data can be transformed into a 1A image. Since the attitude and orbit of the satellite vary continuously and are thus not consistent during imaging, the 1A image contains some geometrical distortion. To compensate for this error, the geometric correction process is then applied, which results in a 1B image.

During geometric correction, the 1A image is compared and matched with a reference image. Convolutional matching shows the extent of location errors in the image. The reference images, obtained from previous imaging, are geometrically corrected and are comprised of shore line edges. These reference images are called landmark images; their locations are well-known and the image size is usually small (128×64). It is, therefore, necessary for the 1A image to be edge-filtered to enable precise matching with landmarks. Conventionally a Sobel or Canny filter is used for this process. Another solution for edge filtering is a neural network approach because it is capable of adaptive learning and non-linear mapping (Lu et al. 2011).

A simple Spiking neural network (SNN) is known to be effective for simulating a visual system since it has a modeling structure that can describe the operation of the human visual system (Wu et al. 2007). It allows for rapid decoding of sensor information, as in the visual system, where massive parallel processing is possible. This neural network can be easily adapted to perform edge detection by adjusting the weight matrices and thresholds. It also has greater potential than other methods for performance improvements through parameter optimization.

This paper introduces a neural network edge detection algorithm that can be applied to satellite meteorological images. Its effectiveness is demonstrated by processing COMS images. The results are then compared with those of conventional methods, and the influences on the accuracy of convolutional matched filtering are discussed.

Received 23 AUG 2016 **Revised** 14 NOV 2016 **Accepted** 15 NOV 2016
†**Corresponding Author**
E-mail: ljh@kari.re.kr, ORCID: 0000-0002-2475-9674
Tel: +82-42-860-2464, Fax: +82-42-860-3909

http://janss.kr pISSN: 2093-5587 eISSN: 2093-1409

2. GEOMETRIC CORRECTION OF SATELLITE IMAGES

When the ground station receives data from COMS MI, the MI images are processed for radiometric and geometric correction. Fig. 1 depicts the overall processes used to create a 1B image from raw data.

After cloud removal, the 1A image is filtered for edge detection. The edged image is then compared and matched with the landmark, while positional errors at the pixel level of the 1A image are evaluated. These error vectors, along with the attitude and orbit information of the satellite, are delivered to the final stage of geometric correction, and the state vector is obtained as the result (NASA/GSFC 1996). The state vector allows for precision resampling of the 1A image and enables a 1B image output that is radiometrically and geometrically corrected. It also facilitates on-orbit sensor calibration when uploaded to the spacecraft and updates of the landmark database.

The most essential process in geometric correction is landmark matching that estimates the positional errors in the 1A image with the cross correlation results of the edged image. The edge detection method involved should ensure accurate and precise extractions of edges since its performance greatly influences the overall quality of the final satellite image.

3. CONVENTIONAL EDGE DETECTION METHODS

The most popular method for image edge detection is the Sobel filter, which is also used in the ground processing of COMS images. The Sobel filter is a kind of a discrete first-order gradient detector that has two 3×3 convolution masks for detecting edges in the horizontal and vertical directions (Lu et al. 2011). After convolving the image with the integer-valued masks to calculate derivatives in both directions, it outputs the pixel values of an edged image by summing or averaging the derivatives. The Sobel filter is a simple solution for edge detection with fewer computational demands, but due to a smoothing effect it provides edges that are several pixels wide (Lu et al. 2011). Wider edges can be a source of error in convolutional matching with landmarks.

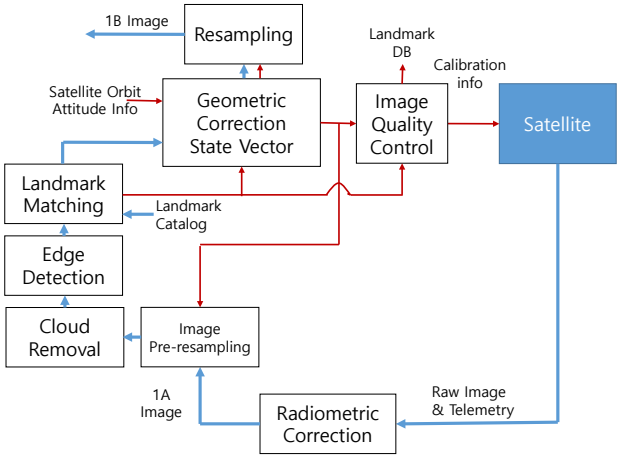

Fig. 1. Functional architecture of MI image correction.

The Canny edge detector is another method that can replace the Sobel filter in this process. The algorithm, introduced in 1986 by J.F. Canny, comprises multiple stages to detect edges in images effectively. The Canny filter first applies Gaussian filtering to remove noise, but not as strongly as the normal smoothing filter, which may wipe out weak edges. It employs an edge detection operator, such as the Sobel operator, to locate the intensity gradients of the image. Non-maximum suppression is applied to thin out the extracted edges in the next stage. By using the double threshold, the spurious edges caused by noise and color variation are eventually suppressed. The final stage enables edge tracking using hysteresis and assesses the connectivity of all edges (Canny 1986). In this process, all the edges that are weak and not connected to a strong edge are eliminated. Although this follows the same process as the Sobel filter, but with larger computational loads; the resulting thinner, connected edges may provide better accuracy in shore line extraction of MI images.

4. NEURAL NETWORK-BASED EDGE DETECTION METHOD

SNN, used in this study for edge detection, was introduced relatively recently. Unlike other traditional neural network models, when all the necessary conditions are met, spiking models have spike outputs, rather than continuously varying outputs (Bogdanov et al. 2009). SNN has been demonstrated to be more plausible than other traditional neural networks, not only because of its biologically inspired parameters, but also because of its use of spatial-temporal information in computation. The temporal information can simply be expressed as the rate of pulsation in SNN (Long & Gupta 2008).

Fig. 2 shows the structure of SNN used in this study. The input layer consists of the neurons that receive the input image; the input gray levels must be normalized to be between 0 and 1. These input values are then delivered to the excitatory

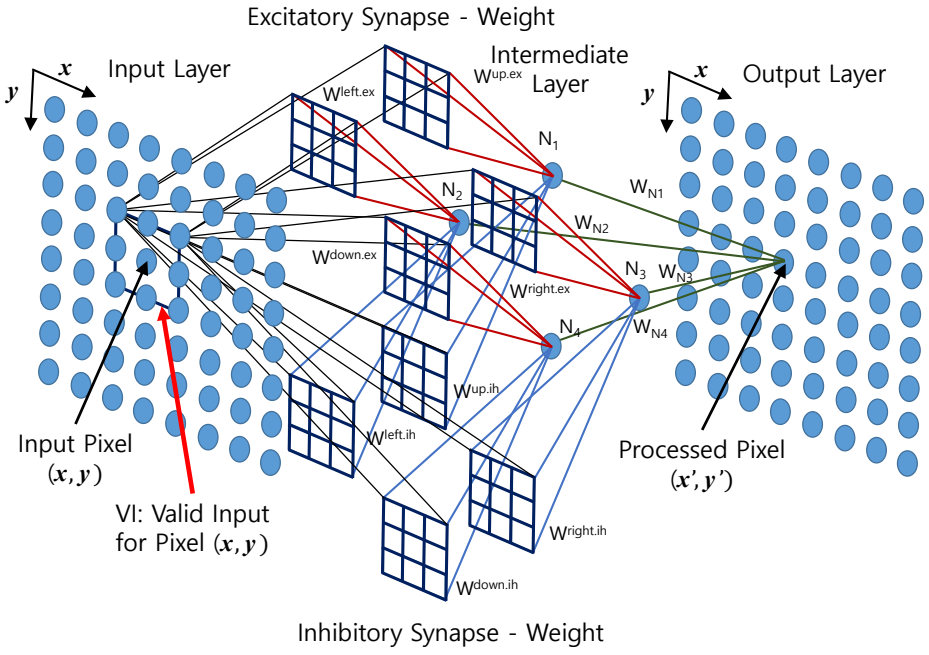

Fig. 2. SNN structure for edge detection.

and inhibitory synapses by the excitatory conductance $g^{ex}_{x,y}$ and the inhibitory conductance $g^{ih}_{x,y}$, respectively, as expressed by Eqs. (1) and (2).

$$\frac{g^{ex}_{x,y}(t)}{dt} = -\frac{1}{\tau_{ex}} g^{ex}_{x,y}(t) + I_{x,y} \tag{1}$$

$$\frac{g^{ih}_{x,y}(t)}{dt} = -\frac{1}{\tau_{ih}} g^{ih}_{x,y}(t) + I_{x,y} \tag{2}$$

where τ_{ex} and τ_{ih} are the constants for excitatory and inhibitory synapses, respectively, and $I_{x,y}$ is the normalized input from the image pixel. Neuron N_1 that is located in the intermediate layer is updated by Eq. (3), using the connected weight matrices.

$$\begin{aligned} C_m \frac{dv_{N1}(t)}{dt} = {} & g_l \left(E_l - v_{N1}(t)\right) \\ & + \sum_{(x,y)\in VI} \frac{W^{up\cdot ex} g^{ex}_{x,y}(t)}{A_{ex}} \left(E_{ex} - v_{N1}(t)\right) \\ & + \sum_{(x,y)\in VI} \frac{W^{up\cdot ih} g^{ih}_{x,y}(t)}{A_{ih}} \left(E_{ih} - v_{N1}(t)\right) \end{aligned} \tag{3}$$

where C_m and g_l are constants representing the capacitance and conductance of neuron N_1, respectively. $v_{N1}(t)$ is the output of neuron N_1. E_l, E_{ex} and E_{ih} are constants involved in the control of momentum, excitatory and inhibitory inputs, respectively. A_{ex} and A_{ih} are constants that adjust the excitatory and inhibitory inputs of neurons, respectively. The connection weight W comprises a 3×3 matrix in which only the patterned boxes in Fig. 2 have nonzero values , and *VI* refers to the valid input region such that the input layer is limited to the same size (3×3), i.e., from (x-1, y-1) to (x+1, y+1).

By Eq. (4), a spike is delivered to the output layer when the output of neuron N_1 exceeds the threshold, v_{th}.

$$\begin{aligned} &\text{if } v_{N1} \geq v_{th}, \text{ then } S_{N1}(t) = 1 \\ &\text{if } v_{N1} < v_{th}, \text{ then } S_{N1}(t) = 0 \end{aligned} \tag{4}$$

where $S_{N1}(t)$ is the series of the output generated by neuron N_1. The output layer is governed by Eqs. (5) and (6) using the weights $W_{N1,\ldots,N4}$ and the input delivered from the intermediate layer.

$$\begin{aligned} \frac{g^{ex}_{x',y'}(t)}{dt} = {} & -\frac{1}{\tau_{ex}} g^{ex}_{x',y'}(t) + (W_{N1}\, S_{N1}(t) + W_{N2}\, S_{N2}(t) \\ & + W_{N3}\, S_{N3}(t) + W_{N4}\, S_{N4}(t)) \end{aligned} \tag{5}$$

$$\begin{aligned} C_m \frac{dv_{x',y'}(t)}{dt} = {} & g_l \left(E_l - v_{x',y'}(t)\right) \\ & + \frac{g^{ex}_{x',y'}(t)}{A_{ex}} \left(E_{ex} - v_{x',y'}(t)\right) \end{aligned} \tag{6}$$

where $g^{ex}_{x',y'}$ is the conductance that transmits the excitatory input to pixel (x',y'). It should be noted that there is no inhibitory input in the output layer. A spike is also generated in the layer when the output of neuron $N_{x',y'}$ exceeds the threshold value. The pulse rate over the given time interval determines the existence of edges in the image. Once any neuron generates a spike, it falls into a refractory state, in which no input is received. After a given period, the neuron is again able to integrate input to generate a spike. All the parameters used in the simulation are consistent with

(a) Lena Image (b) Sobel filter (c) Canny filter (d) SNN filter

Fig. 3. Comparison of the edge detection results.

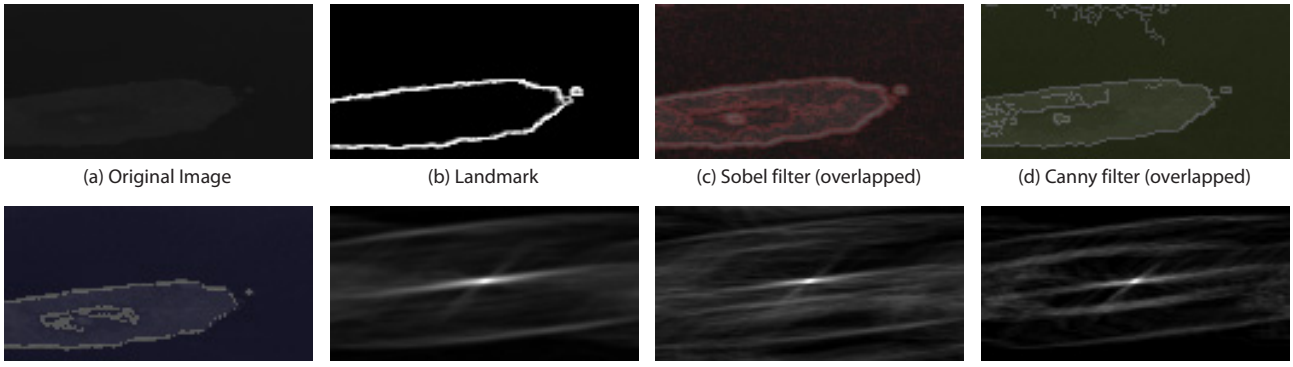

(a) Original Image (b) Landmark (c) Sobel filter (overlapped) (d) Canny filter (overlapped)

(e) SNN filter (overlapped) (f) (b)&(c) matching result (g) (b)&(d) matching result (h) (b)&(e) matching result

Fig. 4. Comparison of the edge detection and matching results on Jeju Island.

values known to be biologically meaningful (Wu et al. 2007), and the values of the weight matrices are evaluated through simulation.

5. SIMULATION RESULTS

The output of the proposed SNN filter was compared with that of the conventional Sobel and Canny filters. The famous "Lena" image was used in order to demonstrate the edge detection capability of all three methods, the results of which are displayed in Fig. 3. Gaussian low pass filtering was applied prior to edge detection in all three cases to reduce noise impact. The output of the Canny filter in Fig. 3 is shown in black and white due to the double threshold, and differs from that of the Sobel, displayed in grayscale. The SNN output is expressed in the form of a spike-pulse rate map of the output layer, where brighter lines mean more spikes than the given threshold. The network was set to iterate 100 times, which is also biologically consistent (Wu et al. 2007).

As shown in Fig. 3, the output of SNN contains many edges, especially in medium-dark areas, whereas it has fewer components in relatively brighter regions. By taking advantage of this feature, the SNN filter may have an advantage in processing MI images, since all lands are relatively dark, and most of the brighter levels are clouds, which have to be removed.

Fig. 4 shows the results of edge detection for an MI image depicting Jeju Island, located southwest of the Korean Peninsula. The COMS MI image was transmitted in March 2013. Only the visible channel data were used for this simulation. Since MI images are huge in scale, it is rather effective to show the results in the actual landmark size (128×64) and then compare them. In Fig. 4, Jeju Island captured from the original MI image is shown in (a), the extracted landmark from (a) is shown in (b), and the edge detection results of all three methods are shown in (c), (d) and (e), respectively, after overlapping each one above the original image. In order to avoid distortion, Gaussian filtering was not applied in all three cases. It is easily observed that due to the smoothing effect, the Sobel filter generates wider edges as apparent in Fig. 4(c), which may be a drawback in the next matching process. The output of the Canny filter, Fig. 4(d), displays narrower edges than that of the Sobel, but contains extraneous components. Correct shore lines are seen in the SNN results, Fig. 4(e), but not all the edges are connected.

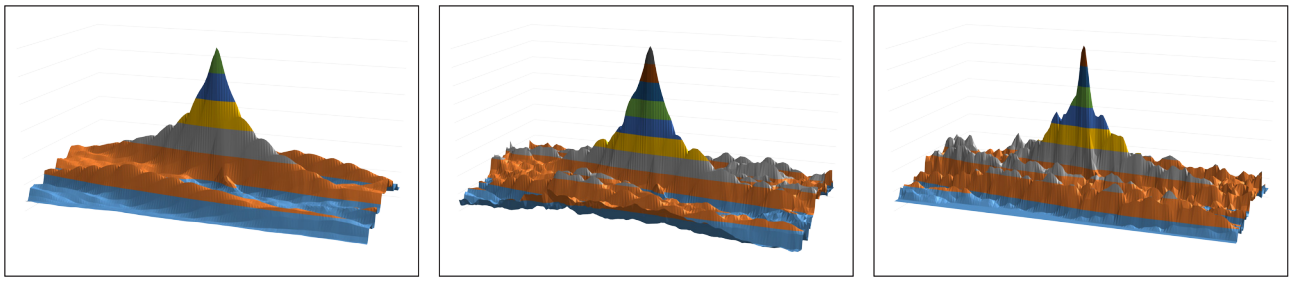

(a) Sobel filter (b) Canny filter (c) SNN filter

Fig. 5. Three-dimensional display of the matching results on Jeju Island.

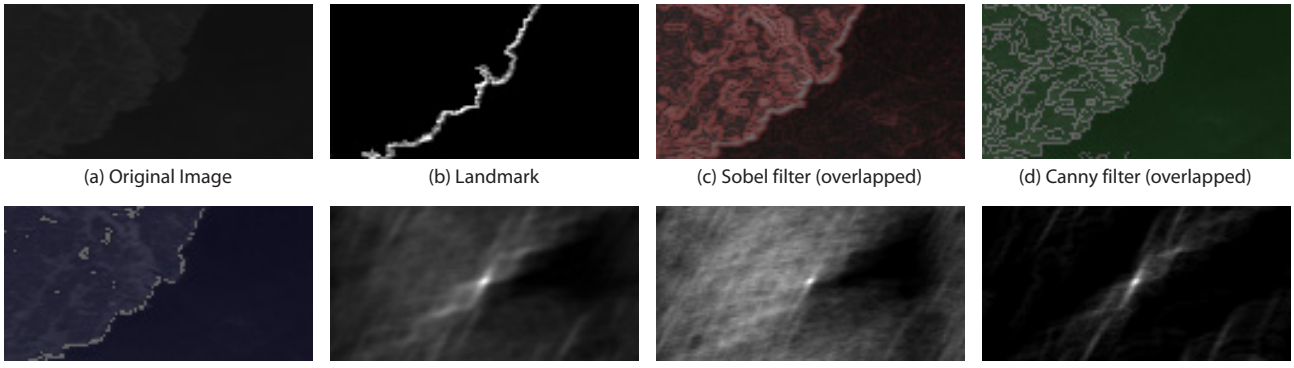

(a) Original Image (b) Landmark (c) Sobel filter (overlapped) (d) Canny filter (overlapped)

(e) SNN filter (overlapped) (f) (b)&(c) matching result (g) (b)&(d) matching result (h) (b)&(e) matching result

Fig. 6. Comparison of the edge detection and matching results on the Ulsan area.

After extracting the edges, frequency domain matching should be done in the COMS ground system to assess the positional error of the observed image. In this process, first, Fourier transform is applied to the edged image, along with the landmark. The frequency domain data of the edged image are then multiplied by the complex conjugate of the Fourier transformed landmark. The final matching result is obtained by applying inverse Fourier transform to the product. The matching results of each method are pictured in 2-D in Figs. 4(e)-4(g). The Sobel output has a broad peak because of its wider edges, whereas that of SNN shows the sharpest peak. This is more obvious in a three-dimensional graph, as shown in Fig. 5. The peak of the Sobel output is so broad that it may cause a higher rate of false alarms when the image is not clear. The Canny edge has a sharper peak than that of the Sobel filter, but it is not as good as that of SNN. The amplitude of the graphs in Fig. 5 should not be an issue, since it depends on the edged image pixel values that can be significantly changed by the quantization threshold applied.

Another simulation result, focusing on the Ulsan area of the Korean Peninsula, is shown in Fig. 6. The peak locations of each matching result are summarized in Table 1, with respect to the sampled areas in this simulation. Table 1 also includes the results for the two cases, Hong Kong and Osaka.

Table 1. Peak locations of the matching results

	Jeju Island	Ulsan	Hong Kong	Osaka
Sobel filter	64, 30 (+1, -1)	63, 31 (0, 0)	63, 31 (0, 0)	63, 31 (0, 0)
Canny filter	64, 30 (+1, -1)	63, 31 (0, 0)	63, 30 (0, -1)	63, 31 (0, 0)
SNN filter	63, 31 (0, 0)	63, 31 (0, 0)	63, 31 (0, 0)	63, 31 (0, 0)

As stated above, the landmarks used in this simulation were extracted from the same 1A image for verification purposes, so the correlation peak should appear at the center (63, 31). Due to the wider edges and unwanted components in their edged images, in some cases the Sobel and Canny filter outputs have slight positional errors as indicated in Table 1. These errors have a negative impact on the accuracy of the calculated state vector and of image resampling in the next stage. Unlike that of the other methods, the outputs of the SNN filter have a sharp peak at the correct position.

6. CONCLUSION

The proposed SNN edge filter yields similar or better performance than the conventional methods as demonstrated through the simulation. Although the connectivity of edges requires further refinement, when the positional errors of images are calculated, the thinner edges without the

smoothing effect provided can be of help. It is also considered to have greater development potential because it can be further optimized by adjusting the weights and parameters and because its functions inside the algorithm can be extended, such as to cloud removal.

One major drawback when any neural network is implemented using conventional computers is heavy computational loads due to the lack of massive parallelism. This is also true for the SNN filter. It uses all the multiple cores of the central processing unit (CPU), and its required running time is a hundred times that of other methods. The computational loads, however, are expected to be dramatically reduced if it is implemented using graphic processing unit (GPU) multi-cores. Once the ground processing software utilizes thousands of GPU cores, the SNN edge detector can be a better choice for improved performance.

ACKNOWLEDGMENTS

This work was supported by the National Meteorological Satellite Centre (NMSC) of the Korea Meteorological Administration (KMA) with the research project "COMS Meteorological Mission Operation Support V".

REFERENCES

Bogdanov I, Mirsu R, Tiponut V, Matlab model for spiking neural networks, Proceedings of the 13th WSEAS conference on systems, Rodos Island, Greece, 22-24 Jul 2009.

Canny J, A computational approach to edge detection, IEEE Trans. Pattern Anal. Mach. Intell. PAMI-8, 679-698 (1986). http://dx.doi.org/10.1109/TPAMI.1986.4767851

Long LN, Gupta A, Biologically-inspired spiking neural networks with Hebbian learning for vision processing, Proceedings of the 46th AIAA Aerospace Science Meeting and Exhibit, Reno, NV, USA, 07-10 Jan 2008.

Lu D, Yu XH, Jin X, Li B, Chen Q, et al., Neural network based edge detection for automated medical diagnosis, Proceedings of the IEEE International Conference on Information and Automation, Shenzhen, China, 6-8 Jun 2011.

NASA/GSFC, GOES I-M DataBook (NASA/GSFC, Greenbelt, 1996).

Wu QX, McGinnity M, Maguire L, Belatreche A, Glackin B, Edge detection based on spiking neural network model (Springer Berlin Heidelberg, Heidelberg, 2007).